Ice or water: thermal properties of monolayer water adsorbed on a substrate

J. Stat. Mech. (2013) P06009

(http://iopscience.iop.org/1742-5468/2013/06/P06009)

Journal of Statistical Mechanics: Theory and Experiment
An IOP and SISSA journal

Ice or water: thermal properties of monolayer water adsorbed on a substrate

Jigger Cheh[1], Yi Gao[1], Chunlei Wang[1], Hong Zhao[2] and Haiping Fang[1]

[1] Shanghai Institute of Applied Physics, Chinese Academy of Sciences, Shanghai 201800, People's Republic of China
[2] Department of Physics, Institute of Theoretical Physics and Astrophysics, Xiamen University, Xiamen 361005, People's Republic of China
E-mail: jigger@sinap.ac.cn, gaoyi@sinap.ac.cn, wangchunlei@sinap.ac.cn, zhaoh@xmu.edu.cn and fanghaiping@sinap.ac.cn

Received 27 February 2013
Accepted 21 May 2013
Published 20 June 2013

Online at stacks.iop.org/JSTAT/2013/P06009
doi:10.1088/1742-5468/2013/06/P06009

Abstract. Adsorbed water molecules on an ionic surface may exhibit an ordered monolayer on the surface. The ordered structure gives it many unique properties that are distinct from either liquid water or ice. We use molecular dynamics simulations to investigate the thermal properties of monolayer water, and find that its thermal conductivity is more similar to ice than to liquid water. The dependence of the thermal conductivity on the charge on the substrate and the temperature are studied. This study explores the density distribution of the water molecules to explain the dependence relations, and examines the effect of bulk water on the structure and thermal properties of monolayer water. Furthermore, kinetic energy transportation in monolayer water is studied.

Keywords: water, aqueous solutions and network-forming liquids, heat conduction, molecular dynamics

Contents

1. Introduction

Adsorbed water on a solid surface is ubiquitous in nature. Understanding its properties is important as it plays a role in many processes, including hydration in biological and colloidal systems [1]; the diffusion of ions in nanopores, biological membranes, and ion channels [2]–[5]; the transformation of solid phases [6]; the interface friction and cloud formation on aerosol particles [7, 8]; and water permeation across nanochannels [9]–[13]. When the water is confined to a few monolayers on top of a substrate, the translational entropy of the water molecules is reduced, yielding a much different behavior compared to that observed in bulk. Recently, monolayer water strongly adsorbed on an ionic substrate has become of significant interest [14]–[27]. The water molecules spread out on the substrate and form a single hydration monolayer at ambient temperature. The ordered structure exhibits many unique properties which are distinctive from either liquid water or ice. For example, instead of resulting in complete wetting, water droplets form atop the monolayer water. The spatial orientation of the water molecules is heterogeneous and they form an ordered hexagonal hydrogen bond network. A theoretical model of the hexagonal monolayer water has been proposed by Wang *et al* [17], [21]–[23], [26]. Later studies investigating ordered monolayer water on different ionic substrates have been reported using both simulations [19]–[21], [24] and experiments [14]–[16], [18, 22, 23]. Since the hexagonal structure of monolayer water resembles ice [28]–[32], it is of interest to determine whether its thermal properties are also ice-like.

In this paper, we perform molecular dynamics (MD) simulations to study the thermal conduction of monolayer water adsorbed on ionic substrates. We found that the thermal conductivity of monolayer water is about 2–3 W m^{-1} K^{-1}, which shows more similarity to ice than to liquid water. The thermal conduction and kinetic energy transportation are chirality dependent rather than isotropic. The dependence relation of the thermal conductivity on the charge on the substrate and the temperature is split into two regions due to the density distribution of water molecules under different conditions. The presence of bulk water somehow breaks the ordered structure of monolayer water. Therefore, liquid-like thermal conductivity can be observed by covering the substrate with thick bulk water.

J. Stat. Mech. (2013) P06009

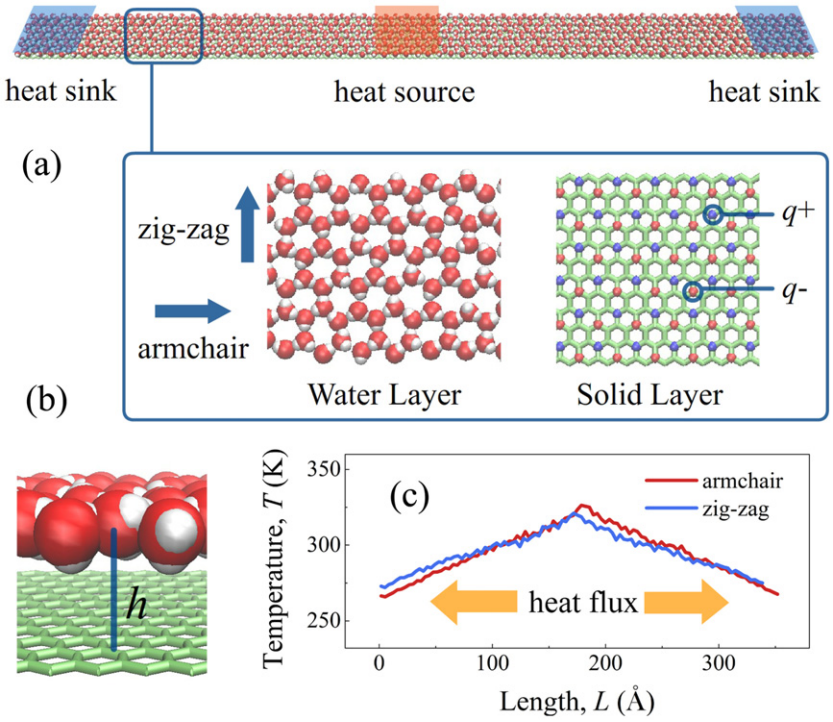

Figure 1. Schematic of monolayer water adsorbed on an ionic substrate. (a) The water molecules (Water Layer) exhibit a hexagonal pattern throughout the surface of the ionic substrate (Solid Layer). The substrate possesses positive charges (q^+, indicated by red balls) and negative charges (q^-, indicated by blue balls). In the thermal conduction process, the hottest water molecules in the left heat sink (covered by the blue square) swap their velocities with the coldest water molecules in the heat source (covered by the orange square). (b) The height of the oxygen atom is labeled as h. (c) The typical temperature profiles of armchair and zig-zag monolayer water. The heat flux runs from the heat source to the heat sink, establishing a steady temperature gradient.

2. Simulation methodology

Monolayer water formation. As a first step, we use MD simulations to obtain ice-like monolayer water adsorbed on an ionic substrate [17, 21, 26] as shown in figure 1(a). The substrate (Solid Layer) possesses positive charges (q^+) and negative charges (q^-), which are assigned to the diagonal atoms in the neighboring hexagons. The water molecules are adsorbed on the surface due to the charges. By carefully removing the extra water molecules on top of the monolayer, we obtain the configuration (Water Layer) for the thermal conduction process. Two typical chiralities in the hexagonal pattern are considered: armchair and zig-zag.

Thermal conduction process. Two-dimensional water structures may exhibit slow relaxation [27], therefore we apply a relaxation time of at least 1 ns so as to thermalize the monolayer water to a given temperature, e.g., 300 K. The ordered hexagonal pattern is equilibrated and the dipole orientation of the water molecules is stable and time invariant in several preferential directions (see figures 5(b) and (c) below). Next, we perform thermal

J. Stat. Mech. (2013) P06009

conduction by using the Müller-Plathe algorithm, which is sometimes called a reverse nonequilibrium molecular dynamics (RNEMD) algorithm [33, 34]. A schematic for the RNEMD algorithm is shown in figure 1(a). The monolayer water is divided into 100 slabs, where the first and the last slabs are assigned to be the heat sinks while the middle (51st) slab is the heat source. The hottest water molecules in the first heat sink swap their velocities with the coldest water molecules in the heat source. Over time, it leads to a symmetric temperature profile, which is computed by averaging events over a time interval of 100 ps:

$$T_i(\text{slab}) = \frac{2}{3N_i k_\text{B}} \sum_j \frac{p_j^2}{2m} \tag{1}$$

where $T_i(\text{slab})$ is the temperature of the ith slab, N_i is the number of water molecules in this slab, k_B is the Boltzmann constant and p_j is the momentum of the jth atom in this slab. They typical temperature profiles of armchair and zig-zag monolayer water are shown in figure 1(c).

The thermal conductivity of monolayer water is obtained by considering Fourier's law:

$$\kappa = \frac{J/(W \times H)}{2\mathrm{d}T/\mathrm{d}L} \tag{2}$$

where J is the heat flux transferred between the heat source and the heat sink, W is the width of the monolayer water, H is the height of the monolayer water, and $\mathrm{d}T/\mathrm{d}L$ is the temperature gradient in response to the heat flux. The height of the monolayer water H can be obtained by considering the average height of the water molecules:

$$H = \langle h \rangle \tag{3}$$

where h is the height of the water molecule as shown in figure 1(b). For simplicity, we use the height of the oxygen atoms to represent the height of the water molecules in our considerations. Later we show that the distribution of height h of the water molecules (density distribution) determines the dependence relations of thermal conductivity upon the charge q and temperature T. Therefore, we will discuss the distribution profiles of h in detail in section 3.

Model and simulation details. Two simulation boxes are considered: the first has dimensions $35 \times 2.5 \times 20$ nm^3 with the armchair edge along the length. The second has dimensions $34 \times 2.4 \times 20$ nm^3 with the zig-zag edge along the length. The periodic boundary condition is applied in all directions. Similarly, in the study of thermal conduction of bulk water covered on the substrate, the thickness of the bulk water is about 5 nm. The dimension is $8.8 \times 2.5 \times 5$ nm^3 with the armchair edge along the length. A periodic boundary condition is applied which makes the bulk water actually confined in two solid layers. The interaction between the different atoms takes a similar form, consisting of the contributions from the electrostatic, dispersion, and repulsive forces:

$$E_{ij} = \frac{k_C q_i q_j}{r_{ij}} + 4\varepsilon_{ij}\left[\left(\frac{\sigma_{ij}}{r_{ij}}\right)^{12} - \left(\frac{\sigma_{ij}}{r_{ij}}\right)^{6}\right] \tag{4}$$

where k_C is the electrostatic constant, q_i (q_j) is the charge of the ith (jth) atom, r_{ij} is the distance between the two atoms, and ε_{ij} and σ_{ij} are the associated Lennard-Jones parameters. The TIP3P model is used to simulate water. The Lennard-Jones parameters

J. Stat. Mech. (2013) P06009

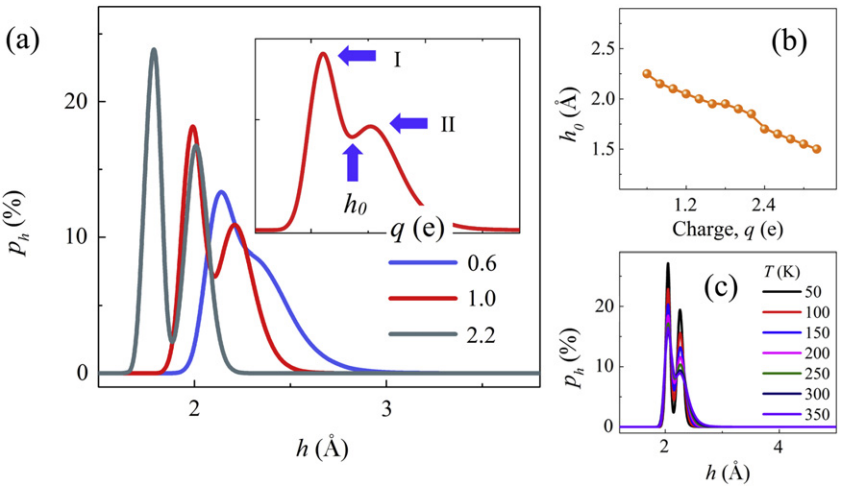

Figure 2. (a) Density distribution of the oxygen atom as a function of its height above the surface. I, II and h_0 indicate the position of the first peak, the second peak, and the first trough in the density profiles, respectively. (b) h_0 as a function of the charge q on the substrate. (c) Density distribution of the oxygen atom for different temperatures T.

between the oxygen atom and atom in the solid layer are $\varepsilon_{so} = 0.01$ kcal mol^{-1} and $\sigma_{so} = 3.2$ Å, and the atoms in the solid layer are fixed. Therefore, the interference of the substrate with the thermal conduction in monolayer water can be neglected. The long-range Coulomb force is evaluated with the PPPM method [35], which splits the long-range effect into short-range and long-range components. A minimum timestep of 1 fs is employed with a velocity-Verlet integration scheme. An open-source package, LAMMPS is used to perform all the MD simulations [36].

3. Results and discussion

First we discuss the density distribution (distribution of height H) of the water molecules. Later we show that this distribution determines the dependence relations of the thermal conductivity upon the charge q and temperature T. The density distribution of the water molecules as a function of the distance from the substrate is:

$$p_h = \frac{N(h)}{\sum_h N(h)} \tag{5}$$

where $N(h)$ is the number of water molecules atop the surface at h.

In figure 2(a), the density distribution is provided for different charges q on the substrate. It is a two-peak distribution, which indicates that even in the same monolayer, the water molecules are not in the exact same plane but are split slightly into two slabs. This is due to the tetrahedral arrangement of the oxygen atom under the sp^3 hybridization. In principle, water molecules are unable to establish a perfect two-dimensional geometry. Here, the two slabs represent two configurations of the water molecules in the ice-like structure, as shown in figure 3. The water molecules have two configurations: State 1 and State 2 [17, 21, 26]. In State 1, both hydrogen atoms are attracted by the oxygen

J. Stat. Mech. (2013) P06009

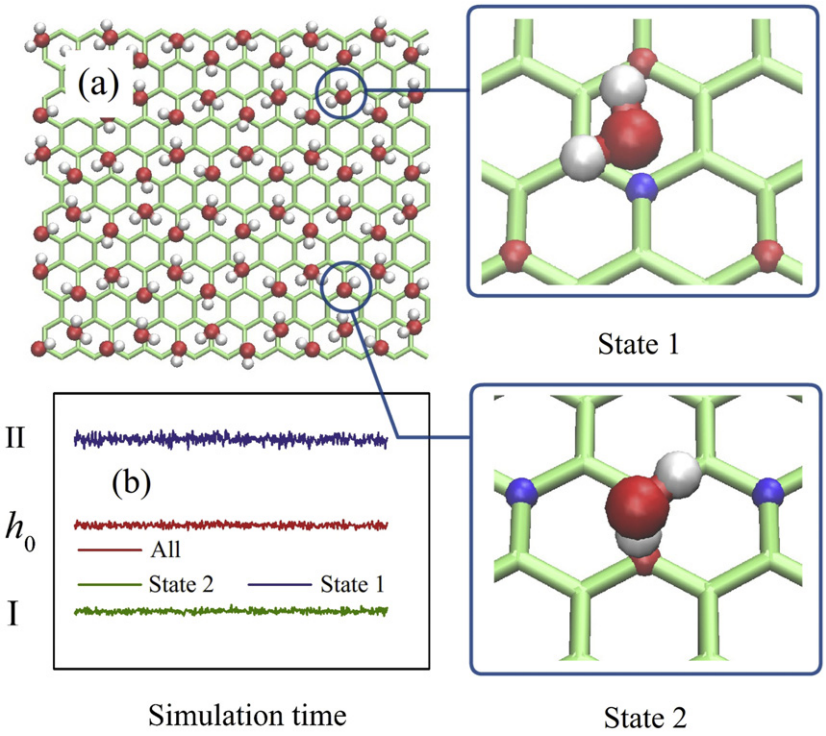

Figure 3. (a) Water molecules form a hexagonal pattern throughout the surface under two configurations. State 1: both hydrogen atoms are attracted by the oxygen atoms of two neighboring water molecules. State 2: one hydrogen atom is attracted by the negative charge on the substrate, and the second is attracted by the oxygen atom in a neighboring water molecule. (b) The average height of all the water molecules, and of the water molecules under State 1 and State 2.

atoms of two neighboring water molecules. In State 2, one hydrogen atom is attracted by the negative charge on the substrate, and the second is attracted by an oxygen atom in the neighboring water molecule. In each hexagon of the monolayer water, three water molecules are under State 1 while the other three are under State 2.

In figure 3(b), the average height of all the water molecules, under State 1 and State 2 is reported as a function of the simulation time. The heights of the water molecules under State 1 and State 2 equal I and II respectively. The height of the monolayer water equals the trough value h_0. This leads to the following relation:

$$H = \langle h \rangle = \frac{(\mathrm{I} + \mathrm{II})}{2} \approx h_0 \tag{6}$$

In figure 2(b), the dependence of h_0 is reported as a function of the charge on the substrate. A larger charge leads to a stronger adsorption of the water molecules on the surface. In figure 2(c), the density distribution of the water molecules is reported for different temperatures. The positions of the peaks and the trough are invariant. Therefore, the height of the monolayer water is variable with q and invariant with T.

Next, we obtain the thermal conductivity of monolayer water according to equation (2). In figure 4(a), we report the thermal conductivity κ as a function of charge q in armchair and zig-zag monolayer water. In the actual ionic substrate models,

J. Stat. Mech. (2013) P06009

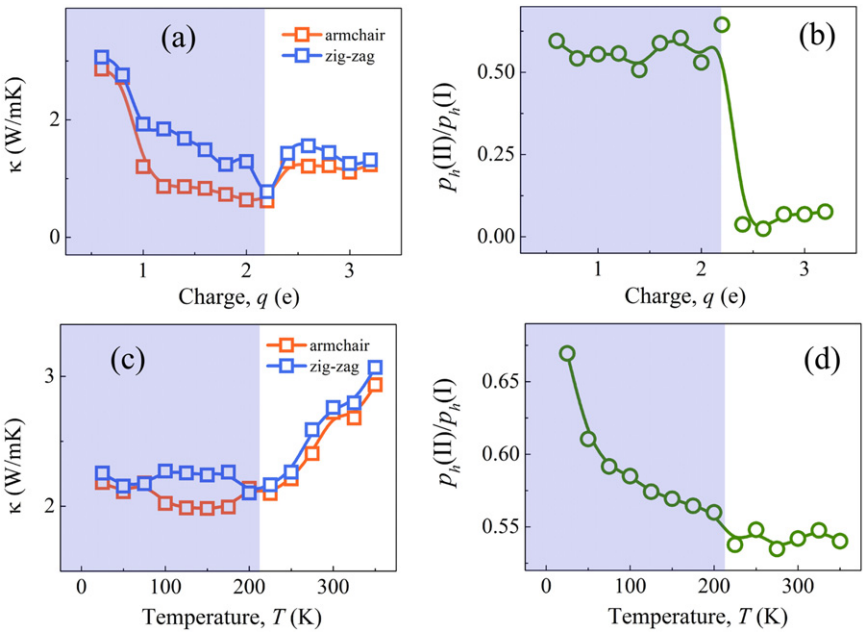

Figure 4. Thermal conductivity of monolayer water. (a) Thermal conductivity κ and (b) the peak ratio $p_h(\mathrm{II})/p_h(\mathrm{I})$ as a function of charge q on the substrates. (c) Thermal conductivity κ and (d) the peak ratio $p_h(\mathrm{II})/p_h(\mathrm{I})$ as a function of temperature T.

the atomic charges are usually fitted by using the electron density fitting method from density-functional theory. For example, the atomic charges of B (boron) and N (nitrogen) are $\pm 0.93e$, those of Mg and O are $\pm 1.2e$, and those of Si and C are $\pm 1.4e$ [37]–[39]. Therefore, a large value range in the MD simulations is considered to predict the properties of monolayer water on new materials.

Figure 4(a) implies several properties of monolayer water: (1) the thermal conduction process is chirality dependent. Higher thermal conductivity is always observed in the zig-zag direction. Similar preferential thermal conduction has also been observed in other hexagonal materials, such as graphene and carbon nanotube. It indicates that the phonon scattering in monolayer water is also chirality dependent [40]–[42]. (2) Thermal conductivity of the monolayer water is similar to ice (2.2 W m^{-1} K^{-1} at 275 K [43]) for a small charge value (0.6–0.8e). (3) The dependence relation exhibits two regions with different thermal behaviors. In the first region, covered by the blue square, the thermal conductivity decreases with the charge q. In the latter region, the thermal conductivity rises dramatically.

We consider the peak ratio $p_h(\mathrm{II})/p_h(\mathrm{I})$, which represents the structure of monolayer water, in order to understand the dependence relation of the thermal conductivity. Figure 4(b) shows the peak ratio to be a function of charge q. Two regions are observed. In the first region, covered by the blue square, the ratio fluctuates around 0.5. The hexagonal pattern is stable if the charge is not too large ($q \leq 2.2e$). However, the second peak almost disappears in the second region. For a very large charge ($q \geq 2.4e$), the water molecules deviate from hexagons and the ice-like structure is destroyed. Therefore, the change in the structure leads to different thermal behaviors in monolayer water.

J. Stat. Mech. (2013) P06009

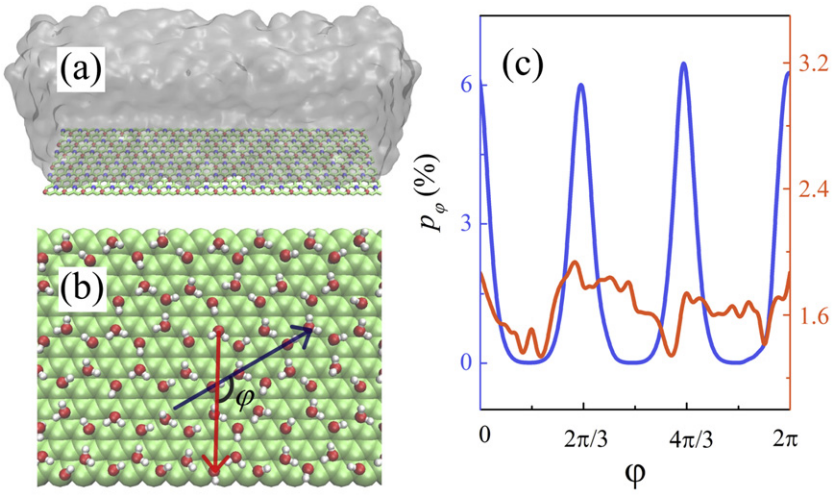

Figure 5. (a) Schematic of bulk water on the ionic substrate. (b) The dipole orientation of a water molecule is represented by the angle φ, where the gray arrow indicates the crystallographic direction and the orange arrow indicates the dipole vector of the water molecule. (c) Distribution of the dipole orientation of monolayer water in the absence of bulk water (blue line) and in the presence of bulk water (orange line).

Figure 4(c) reports the thermal conductivity κ as a function of temperature T. Similar properties are implied. (1) Zig-zag monolayer water always exhibits higher thermal conductivity. (2) The thermal conductivity of monolayer water is similar to ice under various temperatures. (3) The dependence relation exhibits two regions with different thermal behaviors. Similarly, in figure 4(d), the peak ratio $p_h(\mathrm{II})/p_h(\mathrm{I})$ as a function of the temperature T also exhibits two distinct regions, which correspond to two different thermal behaviors. In the first region, the peak ratio decreases with temperature, which indicates that the vibration of the water molecules in the first slab weakens faster than that in the second slab at a lower temperature. In the second region, the ratio fluctuates about 0.5, which indicates that the vibrations in both slabs strengthen at the same rate under a higher temperature.

As a comparison, we also consider the thermal conduction of bulk water on the ionic substrate, as shown in figure 5(a). The momentum exchange of water molecules is performed in the whole bulk water system, and the thermal conductivity is measured by considering the whole bulk water system. This thermal conductivity, which includes the ordered monolayer and the additional liquid atop the substrate, is about 0.8 W m^{-1} K^{-1}. It is similar to the thermal conductivity of liquid water (0.6–0.7 W m^{-1} K^{-1} at room temperature [44]). Therefore, the thermal properties of bulk water are liquid-like rather than ice-like. There are two reasons contributing to the liquid-like thermal conductivity of bulk water: (1) compared with the liquid, the ordered monolayer only accounts for a small portion of bulk water. Therefore, the thermal conductivity of bulk water is affected more by the liquid. (2) The presence of the liquid somehow breaks the ordered structure of monolayer water. In order to illustrate how this ordered structure is damaged by the liquid, we consider the dipole orientation distribution of water molecules [17], [21]–[23], [26].

J. Stat. Mech. (2013) P06009

As shown in figure 5(b), the dipole orientation of water molecules is represented by the angle φ, the angle formed between the projection on the x–y plane of a water molecule dipole orientation (the orange arrow) and the crystallographic direction (the gray arrow). The dipole orientation distribution shows the extent of order/disorder in the hexagonal pattern in monolayer water. The dipole orientation distribution is defined as:

$$p_\varphi = \frac{N(\varphi)}{\sum_\varphi N(\varphi)} \tag{7}$$

where N_φ is the number of water molecules with the dipole orientation angle φ. Figure 5(c) shows the dipole orientation distribution of monolayer water without the liquid part (the blue line, in the absence of bulk water) and with the liquid part (the orange line, in the presence of bulk water). The distribution shows that the preferential dipole orientation has clear peaks at $\varphi = 0$, $\frac{2}{3}\pi$, and $\frac{4}{3}\pi$ in monolayer water in the absence of the liquid part, and has greatly weakened peaks in the presence of the liquid part. Therefore, the liquid part of bulk water is dominant and reduces the impact of the ordered monolayer water, which consequently leads to the liquid-like thermal conductivity in bulk water.

Furthermore, we investigate kinetic energy transportation in monolayer water. A schematic is shown in figure 6. The basic idea is to add a high-energy kick in the center of monolayer water, then after a time period to observe the kinetic energy difference between the current monolayer water and the initial monolayer water without the excitation [45, 46]. The kinetic energy difference represents the transportation ability of thermal energy in different directions.

Here we use 14×14 nm^2 monolayer water which is first thermalized to a very low temperature. Then, we add excited kinetic energy to the center region with diameter of 1.1 nm. The excitation is realized by the generation of velocities in the water molecules that belong to the center region to 300 K. At a given time t, the kinetic energy of a water molecule at position r in the excited system is labeled as $E_{\text{ext}}(r,t)$. At the same time, the kinetic energy of a water molecule in the same position in another system (without excitation, starting from the same initial condition) is labeled as $E_0(r,t)$. Therefore, the kinetic energy transportation density is defined as:

$$\rho_{\text{ext}}(r,t) = \frac{\langle E_{\text{ext}}(r,t) - E_0(r,t)\rangle}{\langle \int_s E_{\text{ext}}(r,t) - E_0(r,t)\,\mathrm{d}s\rangle} \tag{8}$$

where $\langle\rangle$ stands for the average value obtained by independent simulations. Here 35×2 independent simulations (one with excitation and another one without excitation) are carried out to obtain the results. In figure 6, we show $\rho_{\text{ext}}(r,t)$ as a function of simulation time t. The outer edge of the transportation density roughly exhibits a hexagonal pattern in monolayer water. Therefore, the ability to transport thermal energy is anisotropic in monolayer water. This provides another explanation of the chirality dependent thermal conductivity observed in figures 4(a) and (c).

4. Conclusion

MD simulations are performed to investigate the thermal properties of monolayer water adsorbed on a substrate. Due to its ordered hexagonal structure, the thermal conductivity of monolayer water is numerically similar to that of ice. The thermal conductivity of

J. Stat. Mech. (2013) P06009

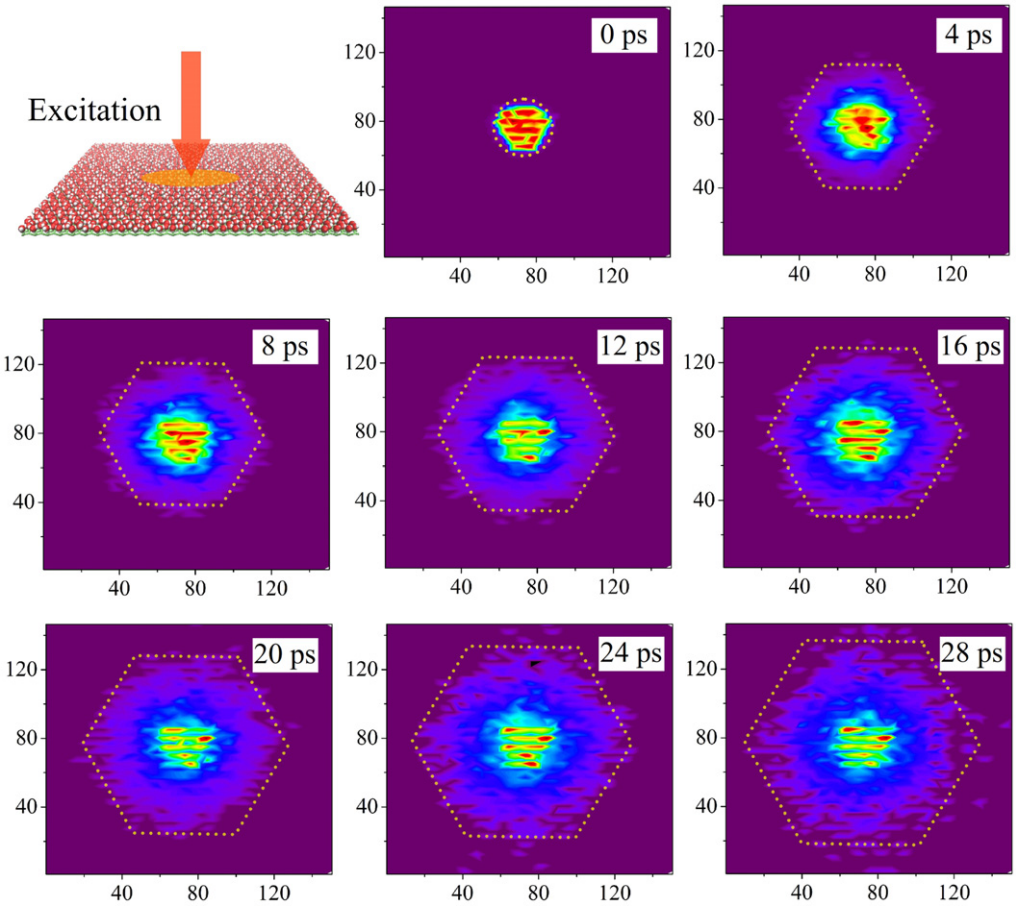

Figure 6. Kinetic energy transportation density $\rho_{\text{ext}}(r,t)$ as a function of time in monolayer water. The center of the monolayer water is excited and the outer edge of the excitation is indicated by dotted lines.

monolayer water and its kinetic energy transportation are anisotropic. In contrast, the thermal conductivity of bulk water on an ionic substrate is numerically similar to that of liquid water, as the impact of the ordered monolayer water can be neglected. Our study indicates that the ice-like structure leads to ice-like thermal behavior in monolayer water and this characteristic should be considered by studying interfacial water related phenomenon.

Acknowledgments

This work was supported by National Natural Science Foundation of China under Grant No. 11290164, 10925525 and 11204341, the 'Hundred People Project' from Shanghai Institute of Applied Physics, Chinese Academy of Sciences, and Shanghai Committee of Science and Technology under Grant No. 11DZ1500400. The authors thank the High Performance Computing and Data Center, Shanghai Advanced Research Institute, Chinese Academy of Sciences.

J. Stat. Mech. (2013) P06009

References

[1] Israelachvili J and Wennerström H, 1996 *Nature* **379** 219
[2] Jiang Y, Lee A, Chen J, Cadene M, Chait B T and MacKinnon R, 2002 *Nature* **417** 515
[3] Fornasiero F, Park H G, Holt J K, Stadermann M, Grigoropoulos C P, Noy A and Bakajin O, 2008 *Proc. Natl Acad. Sci. USA* **105** 17250
[4] Argyris D, Cole D R and Striolo A, 2010 *ACS Nano* **4** 2035
[5] Ho T A, Argyris D, Cole D R and Striolo A, 2012 *Langmuir* **28** 1256
[6] Tardos G I, Nicolaesu I V and Ahtchi-Ali B, 1996 *Powder Handl. Process* **8** 1
[7] Kietzig A-M, Hatzikiriakos S G and Englezos P, 2010 *J. Glaciol.* **56** 473
[8] Pruppacher H R and Klett J D, 1997 *Microphysics of Clouds and Precipitation* (Dordrecht: Kluwer Academic)
[9] Li S, Xiu P, Lu H, Gong X, Wu K, Wan R and Fang H, 2008 *Nanotechnology* **19** 105711
[10] Gong X, Li J, Zhang H, Wan R, Lu H, Wang S and Fang H, 2008 *Phys. Rev. Lett.* **101** 257801
[11] Xiu P, Zhou B, Qi W, Lu H, Tu Y and Fang H, 2009 *J. Am. Chem. Soc.* **131** 2840
[12] Gu W, Zhou B, Geyer T, Hutter M, Fang H and Helms V, 2011 *Angew. Chem. Int. Edn.* **50** 768
[13] Lu H, Gong X, Wang C, Fang H and Wan R, 2008 *Chin. Phys. Lett.* **25** 1145
[14] Spagnoli C, Loos K, Ulman A and Cowman M K, 2003 *J. Am. Chem. Soc.* **125** 7124
[15] Asay D B and Kim S H, 2005 *J. Phys. Chem.* B **109** 16760
[16] Asay D B and Kim S H, 2006 *J. Chem. Phys.* **124** 174712
[17] Wang C, Lu H, Wang Z, Xiu P, Zhou B, Zuo G, Wan R, Hu J and Fang H, 2009 *Phys. Rev. Lett.* **103** 137801
[18] Cardellach M, Verdaguer A, Santiso J and Fraxedas J, 2010 *J. Chem. Phys.* **132** 234708
[19] Argyris D, Ho T, Cole D R and Striolo A, 2011 *J. Phys. Chem.* C **115** 2038
[20] Rotenberg B, Patel A J and Chandler D, 2011 *J. Am. Chem. Soc.* **133** 20521
[21] Wang C, Zhou B, Xiu P and Fang H, 2011 *J. Phys. Chem.* C **115** 3018
[22] James M, Darwish T A, Ciampi S, Sylvester S O, Zhang Z, Ng A, Gooding J J and Hanley T L, 2011 *Soft. Matter.* **7** 5309
[23] James M, Ciampi S, Darwish T A, Hanley T L, Sylvester S O and Gooding J J, 2011 *Langmuir* **27** 10753
[24] Phan A, Ho T A, Cole D R and Striolo A, 2012 *J. Phys. Chem.* C **116** 15962
[25] Wang C, Zhou B, Tu Y, Duan M, Xiu P, Li J and Fang H, 2012 *Sci. Rep.* **2** 358
[26] Wang C, Li J and Fang H, 2011 *Rend. Fis. Acc. Lincei.* **22** S5
[27] Limmer D T, Willard A P, Madden P and Chandler D, 2013 *Proc. Natl Acad. Sci. USA* **110** 4200
[28] Cerdá J, Michaelides A, Bocquet M-L, Feibelman P J, Mitsui T, Rose M, Fomin E and Salmeron M, 2004 *Phys. Rev. Lett.* **93** 116101
[29] Kimmel G A, Matthiesen J, Baer M, Mundy C J, Petrik N G, Smith R S, Dohnálek Z and Kay B D, 2009 *J. Am. Chem. Soc.* **131** 12838
[30] Li H and Zeng X C, 2012 *J. Chem. Theory Comput.* **8** 3034
[31] Choi E-M, Yoon Y-H, Lee S and Kang H, 2005 *Phys. Rev. Lett.* **95** 085701
[32] Jinesh K B and Frenken J W M, 2008 *Phys. Rev. Lett.* **101** 036101
[33] Muller-Plathe F, 1997 *J. Chem. Phys.* **106** 6082
[34] Xiong D, Wang J, Zhang Y and Zhao H, 2012 *Phys. Rev.* E **85** 020102
[35] Darden T, York D and Pedersen L, 1993 *J. Chem. Phys.* **98** 10089
[36] Plimpton S, 1995 *J. Comput. Phys.* **117** 1
[37] Li H and Zeng X C, 2012 *ACS Nano* **6** 2401
[38] Soetens J, Millot C, Hoang P and Girardet C, 1998 *Surf. Sci.* **419** 48
[39] Ma Y and Garofalini S H, 2008 *J. Chem. Phys.* **128** 084505
[40] Hu J, Ruan X and Chen Y P, 2009 *Nano Lett.* **9** 2730
[41] Zhang G and Li B, 2005 *J. Chem. Phys.* **123** 114714
[42] Yamamoto T, Watanabe S and Watanabe K, 2004 *Phys. Rev. Lett.* **92** 075502
[43] Slack G A, 1980 *Phys. Rev.* B **22** 3065
[44] Neindre B L, Bury P, Tufeu R and Vodar B, 1976 *J. Chem. Eng. Data* **21** 265
[45] Zhao H, 2006 *Phys. Rev. Lett.* **96** 140602
[46] Yang J, Zhang Y, Wang J and Zhao H, 2011 *Phys. Rev.* E **83** 052104

J. Stat. Mech. (2013) P06009